

Dislocations in AlGa_N: core structure, atom segregation and optical properties

*Fabien C-P. Massabuau^{*1}, Sneha L. Rhode², Matthew K. Horton³, Thomas J. O'Hanlon¹, András Kovács⁴, Marcin S. Zielinski⁵, Menno J. Kappers¹, Rafal E. Dunin-Borkowski⁴, Colin J. Humphreys¹, and Rachel A. Oliver¹*

¹ Department of Materials Science and Metallurgy, University of Cambridge, Cambridge CB3 0FS, UK

² Department of Materials, Imperial College London, London SW7 2AZ, UK

³ Materials Science and Engineering, University of California Berkeley, Berkeley, CA 94720, US

⁴ Ernst Ruska-Centre for Microscopy and Spectroscopy with Electrons and Peter Grünberg Institute, Forschungszentrum Jülich GmbH, D-52425 Jülich, Germany

⁵ Attolight AG, EPFL Innovation Park, 1015 Lausanne, Switzerland

Abstract

We conducted a comprehensive investigation of dislocations in Al_{0.46}Ga_{0.54}N. Using aberration-corrected scanning transmission electron microscopy and energy dispersive X-ray spectroscopy,

the atomic structure and atom distribution at the dislocation core have been examined. We report that the core configuration of dislocations in AlGa_{0.9}N is consistent with that of other materials in the III-Nitride system. However we observed that the dissociation of mixed-type dislocations is impeded by alloying GaN with AlN, which is confirmed by our experimental observation of Ga and Al atom segregation in the tensile and compressive parts of the dislocations, respectively. Investigation of the optical properties of the dislocations shows that the atom segregation at dislocations has no significant effect on the intensity recorded by cathodoluminescence in the vicinity of the dislocations. These results are in contrast with the case of dislocations in In_{0.09}Ga_{0.91}N where segregation of In and Ga atoms also occurs but results in carrier localization limiting non-radiative recombination at the dislocation. This study therefore sheds light on why InGa_{0.9}N-based devices are generally more resilient to dislocations than their AlGa_{0.9}N-based counterparts.

Keywords

AlGa_{0.9}N, InGa_{0.9}N, dislocation, aberration-corrected TEM, cathodoluminescence.

The III-Nitride system is a very important family of semiconducting materials for light emitting diode (LED) technology. The development of GaN opened the path for efficient LEDs¹. While alloying GaN with InN addresses the question of light emission in the visible spectrum², alloying with AlN paves the way for applications enabled by ultra-violet (UV) light such as water disinfection, skin condition phototherapy, and forensic identification among others³. However, the performance of III-Nitride LEDs varies substantially with the emission

wavelength. Whilst external quantum efficiencies of 84% and 44% can be achieved for blue⁴ and green⁵ LEDs, respectively, that of UV LEDs still remains under 10%³. While InGaN-based devices exhibit a remarkable resilience to high densities of dislocations⁶, dislocations are thought to be a significant factor limiting the efficiency of AlGaIn-based LEDs⁷. It is therefore important to understand the properties of dislocations in AlGaIn and how these may differ from InGaIn.

Dislocations in III-Nitrides fall into three categories depending on their Burgers vector \mathbf{b} , that is, edge-type ($\mathbf{b} = \mathbf{a}$), mixed-type ($\mathbf{b} = \mathbf{a} + \mathbf{c}$) and screw-type ($\mathbf{b} = \mathbf{c}$) dislocations⁸. The atomic structure of the dislocation core in GaN and InGaIn has been the subject of numerous experimental⁹⁻¹⁴ and theoretical¹⁵⁻²¹ investigations because of its potential influence on the formation of mid-gap states which can act as non-radiative recombination centers. In comparison very little is known about dislocations in AlGaIn, and their atomic structure has not been yet reported. The present work aims to conduct a comprehensive study of dislocations in AlGaIn. We thus conducted a statistically meaningful observation of the core structure, of compositional variations, and of the optical behavior of dislocations in AlGaIn. To fully grasp the different impact dislocations may have in AlGaIn and InGaIn alloys, the same analysis was conducted on dislocations in InGaIn.

AlGaIn and InGaIn epilayers were grown by metal-organic vapor phase epitaxy (MOVPE) in a Thomas Swan 6 x 2 inch close-coupled showerhead reactor. Trimethylgallium (TMG), trimethylaluminium (TMA), trimethylindium (TMI), diluted silane in hydrogen (SiH₄) and ammonia (NH₃) were used as precursors for the Ga, Al, In, Si and N elements, respectively. Hydrogen (H₂) was used as carrier gas for the growth of GaN, AlN and AlGaIn, while a mixture of hydrogen and nitrogen (N₂) was employed for the growth of InGaIn.

For the AlGa_xN epilayer, a *c*-plane sapphire substrate was employed. Following the growth of a 30 nm AlN buffer layer at 1050 °C, a 2 μm AlN layer was grown at 1130 °C. A SiN_x interlayer was then deposited to allow for the subsequent growth of faceted GaN islands at 980 °C for 120 s. Finally the 3 μm Al_xGa_{1-x}N epilayer with an Al content of $x \sim 46\%$ was deposited at 1090 °C. X-ray diffraction on a Philips X'Pert MRD diffractometer was used to determine the composition and strain state of the layer. From reciprocal space maps taken on the 004 and 105 reflections, the AlGa_xN layer was found to be 89% relaxed with regard to the strain-free AlN layer. Further details about the growth of the sample can be found in Ref. 22.

For the InGa_xN epilayer, a *c*-plane sapphire substrate was employed. A 5 μm GaN buffer layer (of which 2 μm undoped and 3 μm Si-doped to $5 \times 10^{18} \text{ cm}^{-3}$) was then deposited. Following the growth of an additional 500 nm of GaN, a 135 nm In_xGa_{1-x}N epilayer with an In content of $x \sim 9\%$ was deposited at 749 °C. (This particular composition of InGa_xN was chosen because it has been thoroughly studied previously²³.) From reciprocal space maps taken on the 006 and 204 reflections, the InGa_xN layer was found to be fully strained to the GaN pseudo-substrate. Further details about the growth of the sample can be found in Ref. 23.

Dislocations in the AlGa_xN epilayer were observed by aberration-corrected high-angle annular dark field scanning transmission electron microscopy (HAADF-STEM) using an FEI Titan G2 80-200 ChemiSTEM²⁴ and FEI Titan G3 50-300 PICO²⁵ microscopes operating at 300 kV with a detector collection semi-angle of 69 mrad. The sample was prepared for plan-view TEM imaging using standard mechanical polishing method followed by Ar⁺ ion milling at 5 kV and cleaning from 1 kV down to 0.1 kV. The dislocations were viewed end-on - *i.e.* along the [0001] zone-axis - therefore allowing for the identification of the core structure⁹⁻¹². Eshelby Twist, which is an apparent rotation of the lattice caused by the relaxation of stresses at the free surface caused

by the screw component of a dislocation²⁶, was observed for all mixed-type dislocations. Focal series images for all dislocations reported in this study were visually observed for the Eshelby twist. Eshelby twist was observed in a 1.5 nm × 1.5 nm or larger area around mixed-type dislocation cores, depending on the mixed-type core structure observed. This large displacement of atomic columns was used to distinguish between mixed-type and edge-type dislocations in this study, and in similar previous studies on doped and alloyed GaN⁹⁻¹¹. The composition around the dislocations was investigated by energy dispersive X-ray spectroscopy (EDX) in the FEI Titan G2 80-200 ChemiSTEM microscope. The EDX quantification was based on line scans taken across the dislocation cores, with a *ca.* 1 nm analysis width, and was performed using a standard background subtraction and the Cliff-Lorimer factor method. For statistical validity, over 40 dislocations were observed for core structure identification, and 12 for compositional analysis.

The optical properties of dislocations in AlGaIn and InGaIn were compared using a "multi-microscopy" methodology. As described in Ref. 27, a copper grid for TEM sample preparation was positioned on the surface of the sample using epoxy resin. Using the 50 μm size square mesh of the grid, the same set of dislocations could be examined by atomic force microscopy (AFM) and scanning electron microscopy with cathodoluminescence (SEM-CL). AFM was conducted on a Veeco Dimension 3100 operating in tapping mode and was used to measure the size of pits at the termination of dislocations, which allows one to obtain the dislocation type, and the distance to nearest neighbor, following the procedure described in earlier work²³. It should be noted that in the case of the AlGaIn layer, the dislocations emerging at the surface of the sample are significantly smaller than the V-shaped pits present in InGaIn, hence the pit size was obtained in this sample using the pit depth, instead of the pit width. SEM-CL was conducted

1
2
3 at liquid He (10 K) temperature in an Attolight Rosa 4634 CL microscope for the AlGa_N sample
4
5 and a FEI XL30 microscope equipped with a Gatan Mono CL4 CL system for the InGa_N
6
7 sample. The AlGa_N and InGa_N samples exhibited a CL peak emission wavelength at 279 nm
8
9 (recorded over the 210-345 nm range) and 398 nm (recorded over the 360-425 nm range),
10
11 respectively. The SEMs were operated at 3 kV, resulting in the majority of the CL signal
12
13 collected arising from the first 25-30 nm of material below the surface. This value was confirmed
14
15 using Monte Carlo simulations²⁸, taking into account the absorption coefficient of the
16
17 materials²⁹. SEM-CL was used to analyze the variation in CL intensity and emission energy at
18
19 and around the dislocations. This study was conducted at liquid He temperature (10 K) as it
20
21 significantly increases the intensity of the CL signal, hence allowing the recording of spectral
22
23 maps with a high spectral resolution, here of the order of 1-2 meV.
24
25
26
27
28
29
30
31
32
33
34
35
36
37
38
39
40
41
42
43
44
45
46
47
48
49
50
51
52
53
54
55
56
57
58
59
60

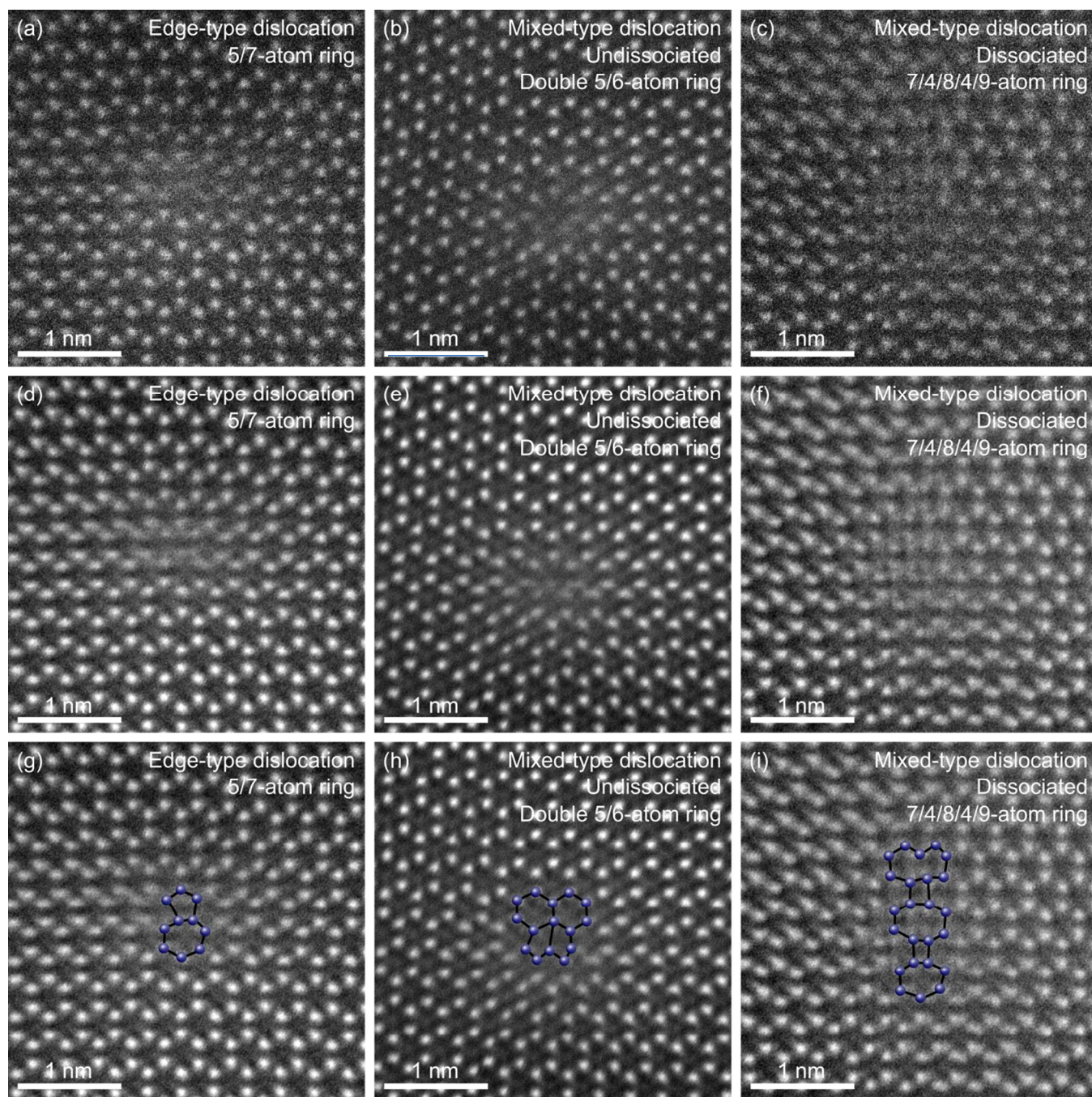


Figure 1. Plan-view aberration-corrected HAADF-STEM image of the AlGaIn sample, showing the core structure of an edge-type dislocation (5/7-atom ring)(a,d,g), an undissociated mixed-type dislocation (double 5/6-atom ring)(b,e,h) and a dissociated mixed-type dislocation (7/4/8/4/9-

atom ring)(c,f,i). Raw unfiltered images (a-c), and ABSF-filtered (average background subtraction filter) (d-f) with atomic columns identified to guide the eye (g-i).

The core structure of the dislocations in the AlGaN sample has been observed by plan-view aberration corrected HAADF-STEM, and three representative examples are shown in Figure 1. Akin to other studies performed on GaN^{9,10} and InGaN^{11,23}, we observed that 100% of the edge-type dislocations form 5/7-atom ring cores, as illustrated in Figure 1(g). In the context of mixed-type dislocations, we observed essentially two different configurations, *i.e.* dissociated and undissociated core structures. In line with previous reports we observed that the undissociated core of mixed-type dislocations form a double 5/6-atom ring (Figure 1(h))^{9,12}. (The undissociated core structure shown could either be an 8-atom or a double 5/6-atom ring. A sub-nm spatial resolution would be required to distinguish between the two configurations. However the energy of the double 5/6-atom configuration was calculated to be lower than that for 8-atom ring in GaN films¹⁵, so it is likely that the core structure in Figure 1(h) is a double 5/6-atom ring.) The dissociated cores correspond to two partial dislocations with Burgers vector $\mathbf{b} = 1/2(\mathbf{a}+\mathbf{c}) = 1/6[1-213]$ connected by a stacking fault with a displacement vector $\mathbf{R} = 1/6[1-213]$, which results in an elongated core as illustrated by Figure 1(i)^{9,12}. The length of the core, that is, essentially the number of 4/8 rings in the core, can vary from dislocation to dislocation. In this sample, cores forming 7/4/9, 7/4/8/5, 7/4/8/4/9, and 7/4/8/4/8/5 atom rings have been observed.

Table 1. Summary of the proportion of dislocation core configurations for a variety of III-Nitride alloys. LDD stands for low dislocation density (*i.e.* $\sim 3 \times 10^8 \text{ cm}^{-2}$) and HDD stands for high dislocation density (*i.e.* $\sim 6 \times 10^9 \text{ cm}^{-2}$).

Alloy	Doping	TD density	Edge 5/7 atom ring	Mixed Undissociated	Mixed Dissociated	Ref.
GaN	Undoped	LDD	100 %	$50 \pm 5 \%$	$50 \pm 5 \%$	9
GaN	Undoped	HDD	100 %	$50 \pm 5 \%$	$50 \pm 5 \%$	9
GaN	Mg	HDD	100 %	$85 \pm 3\%$	$15 \pm 3 \%$	9
GaN	Si	LDD	100 %	$48 \pm 9 \%$	$54 \pm 9 \%$	10
GaN	Si	HDD	100 %	$57 \pm 3 \%$	$43 \pm 3 \%$	10
In _{0.06} Ga _{0.94} N	Si	LDD	100 %	$46 \pm 5 \%$	$54 \pm 5 \%$	11
In _{0.20} Ga _{0.80} N	Si	LDD	100 %	$43 \pm 6 \%$	$57 \pm 6 \%$	11
Al _{0.46} Ga _{0.54} N	Undoped		100 %	$68 \pm 9 \%$	$32 \pm 9 \%$	This work

Table 1 summarizes the data obtained from this experiment and compares them with results available in the literature for a range of III-Nitride alloys. It appears clearly that the dislocation core structures in AlGaN are consistent with those in other nitride alloys under various conditions of composition, dopant type, or dislocation density. The main notable difference lies in the ratio of dissociated to undissociated mixed-type dislocations, which relates to the elastic strain energy around the dislocation core, and has been used in the past to hint at the segregation of solute species around the dislocation⁹. (We note that In atoms were shown to segregate at dislocations in InGaN despite not exhibiting a meaningful change in the ratio of dissociated to undissociated mixed-type dislocations¹¹. This is perhaps because these samples were Si-doped,

1
2
3 and that Si segregation at dislocations inhibits dislocation climb, as was reported in GaN¹⁰.) In
4
5 our AlGaIn sample we can see that the proportion of mixed-type dislocations that dissociate
6
7 deviates from the case of undoped GaN, which indicates that alloying with AlN impedes
8
9 dislocation dissociation. This is in line with Chen *et al.*, who used first principle density
10
11 functional theory calculations to estimate the stability of stacking faults in Mg- and Al-doped
12
13 GaN over the entire compositional range, and predicted that, at comparable composition, Al
14
15 around threading dislocations would hinder dislocation dissociation, but to a much lesser extent
16
17 than Mg³⁰. However, Table 1 compares Al and Mg compositions which are several orders of
18
19 magnitude different - 46% and << 0.1% for Al and Mg respectively. Therefore the results from
20
21 this theoretical work are not directly transferrable to our study, yet it is worth pointing out that
22
23 Table 1 shows that Mg-doped GaN exhibits the lowest proportion of dislocation dissociation,
24
25 followed by AlGaIn. A lower proportion of dislocation dissociation can be attributed to virtually
26
27 any factor that may affect the energies involved in the formation of a dissociated core, that is, the
28
29 elastic strain energy of the dislocation, the stacking fault energy, or the dislocation core energy.
30
31 Given that dislocations in AlGaIn do not seem to differ from other III-Nitrides alloys - as far as
32
33 the core structure is concerned - and that Mg and In have been previously found to segregate
34
35 around the dislocations, consequently reducing the elastic strain energy^{9,11,23,31}, it is appropriate
36
37 to investigate whether similar non-uniformities are seen in the distribution of Al and Ga atoms in
38
39 the vicinity of dislocations in AlGaIn.
40
41
42
43
44
45
46
47
48
49
50
51
52
53
54
55
56
57
58
59
60

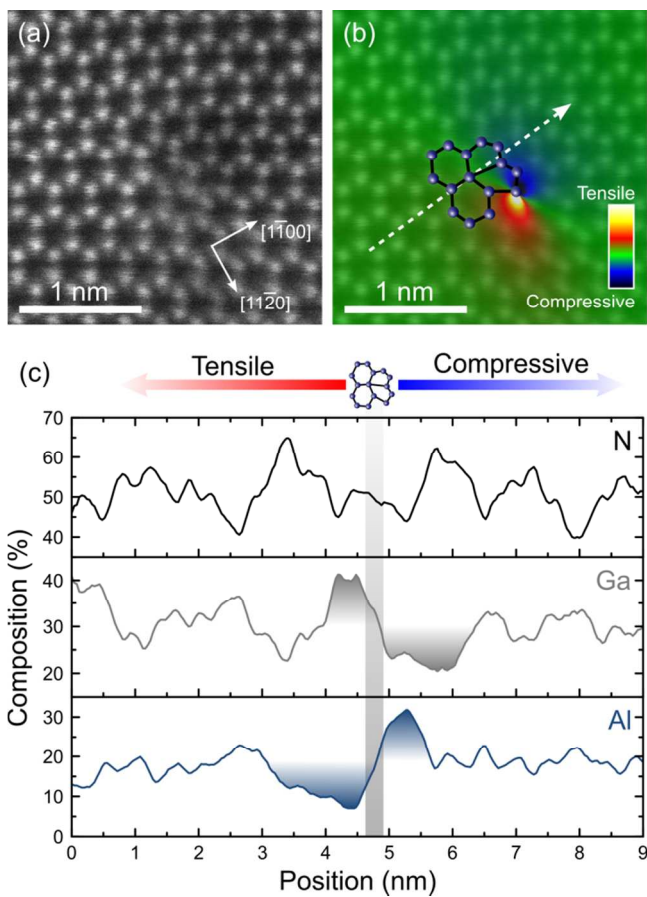


Figure 2. (a) Unfiltered HAADF-STEM image of an undissociated mixed-type dislocation. (b) ABSF-filtered image of (a) with geometric phase analysis overlay showing the x-x strain component (x-axis parallel to [11-20]). (c) EDX line scan showing the composition of Al, Ga, and N along the line depicted in (b) (with a *ca.* 1 nm analysis width).

EDX mapping of dislocations has been conducted inside the TEM. This enabled us to investigate potential connections between the dislocation type and core configuration (obtained through the HAADF-STEM images) to the strain distribution around the dislocation (obtained through geometric phase analysis of the HAADF-STEM images) and to the distribution of Al and Ga atoms around the dislocation (obtained through the EDX map). This is illustrated in

Figure 2 for an undissociated mixed-type dislocation. The geometric phase analysis overlay (here used qualitatively only) shows that the dislocation core is bounded on either side by a region of compressive strain and a region of tensile strain, as expected by the elasticity theory of dislocations. (We also note an asymmetry of the geometric phase analysis map, presumably ascribable to Eshelby twist²⁶). An EDX line scan taken across the dislocation core and from the tensile side to the compressive side, as illustrated in Figure 2(b), reveals the compositional fluctuations around the dislocation. It can be seen in Figure 2(c) that the dislocation core is bounded by a Ga-rich (or Al-poor) region and an Al-rich (or Ga-poor) region (this is particularly noticeable on the Al trace). The segregation of species occurs in close vicinity of the core, on a length scale of about 1-2 nm. The region of higher Ga content is found to relate to the side of the dislocation under tensile strain, whilst the region of higher Al content relates to the side under compressive strain. This is explained by the Al-N bond being shorter than the Ga-N bond³² (in a relaxed $\text{Al}_{0.5}\text{Ga}_{0.5}\text{N}$ alloy, valence force field simulations predicted the Al-N bond to be about 2% shorter than Ga-N), which leads to a reduction of the elastic strain around the dislocation if Ga and Al segregate at the tensile and compressive side of the dislocation, respectively. Our experimental observation agrees with Sakaguchi *et al.* who used empirical interatomic potentials and Monte Carlo simulations to study alloy segregation at dislocations in $\text{Al}_{0.3}\text{Ga}_{0.7}\text{N}$, and found that Ga and Al atoms segregate in the tensile and compressive part, respectively, of dislocations with an edge component³³. We observed similar results irrespectively of the dislocation core configuration, *i.e.* edge, mixed undissociated, mixed dissociated (no screw dislocations were investigated here). This result is consistent with our earlier finding that mixed-type dislocations in AlGa_{0.5}N do not dissociate to as great an extent as in GaN. The segregation of Al and Ga atoms reduces the elastic strain of the dislocation, therefore reducing the driving force for dissociation.

The phenomenon of atom segregation at dislocations has also been reported in InGaN alloys^{11,31} and has been shown to affect the carrier recombination at the dislocation²³. In the case of InGaN, we have suggested that the segregation of In atoms promotes the formation of In-N-In chains and atomic condensates in the tensile part of the dislocation core, which strongly localizes holes³⁴⁻³⁶, and consequently limits non-radiative recombination at the dislocation core. Since dislocations in AlGaN are surrounded by an Al-rich region and a Ga-rich region, it is sensible to consider the possibility that these may alter the carrier recombination in the vicinity of the dislocation.

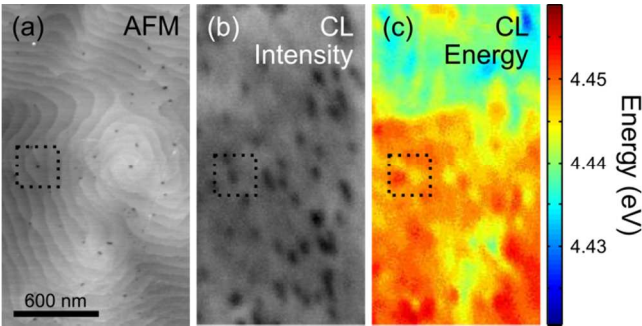


Figure 3. (a) AFM, (b) CL integrated intensity, and (c) CL peak emission energy of the same region in the AlGaN sample.

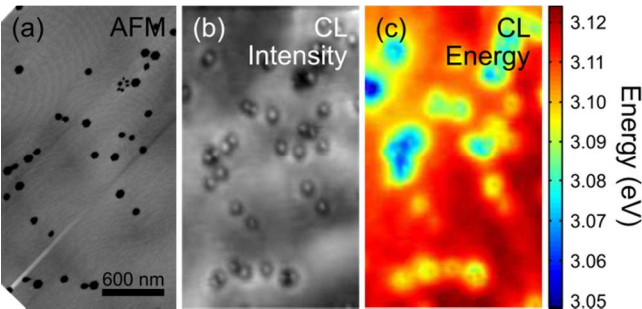


Figure 4. (a) AFM, (b) CL integrated intensity, and (c) CL peak emission energy of the same region in the InGaN sample.

1
2
3 In order to investigate whether the segregation of species reported above has any effect on the
4 optical properties of the dislocations, a multi-microscopy approach based on the combined
5 analysis of AFM, SEM and CL data recorded at liquid He temperatures, has been employed on
6 the AlGa_N sample and is illustrated in Figure 3. For comparison, the same approach under
7 similar experimental conditions has been employed on the InGa_N sample and is presented in
8 Figure 4. The dislocations are readily observable by AFM as they appear at the surface of the
9 sample, as small pits in AlGa_N (Figure 3(a)), and as larger V-shaped pits in InGa_N (Figure 4(a)).
10 A one-to-one correlation can be found between the dislocations identified in the AFM and the
11 dark spots observed on the CL intensity map (Figure 3(b)), which highlights the non-radiative
12 behavior of the dislocations in AlGa_N. This result, although in agreement with the classical
13 picture of dislocations in semiconductors, including GaN³⁷⁻³⁹, deviates strongly with what can be
14 observed in InGa_N. As can be seen in Figure 4(b), the dislocations in InGa_N appear in the CL
15 intensity image as a bright spot surrounded by a dark halo. In our earlier work, this bright spot
16 has been linked to the carrier localization deriving from the segregation of In atoms at the
17 dislocation²³. Previous studies investigating carrier dynamics in thick AlGa_N epilayers reported
18 that excitons were localized at low temperature at compositional fluctuations in the alloy⁴⁰⁻⁴².
19 The CL data presented in Figure 3(b) suggest that if carriers are localized in the vicinity of the
20 dislocations due to the atom segregation, the effect on the CL emission intensity is very limited
21 in contrast to what is observed in InGa_N. This corroborates experimental³⁴ and theoretical³⁵
22 studies which showed that carrier localization induced by In atoms is much stronger than carrier
23 localization from Ga or Al atoms. This result may provide an explanation for the relative
24 resilience of InGa_N-based devices to dislocations, as opposed to AlGa_N-based. We could thus
25 hypothesize that doping AlGa_N with In may be an interesting way to enhance radiative
26
27
28
29
30
31
32
33
34
35
36
37
38
39
40
41
42
43
44
45
46
47
48
49
50
51
52
53
54
55
56
57
58
59
60

1
2
3 recombination at dislocations, as the In atoms may segregate in the tensile part of the
4 dislocations and (strongly) localize carriers.
5
6

7
8 The CL peak emission energy map for the two alloys is presented in Figures 3(c) and 4(c). As
9 reported previously in InGaN, the emission energy corresponding to the bright spot is redshifted
10 compared to that of the surrounding material far away from the dislocation, in agreement with
11 the presence of In-N-In chains and atomic condensates localizing carriers at the dislocation²³.
12
13 Conversely, in AlGaN, the dislocations are bounded on either side by a redshifted and a
14 blueshifted region, as illustrated by the dislocation inside the dotted square in Figure 3. For
15 dislocations which are isolated, that is, typically more than 150 nm away from the nearest
16 neighbouring dislocation, the energy shifts of these regions relative to the emission energy at the
17 dislocation position is very symmetric, with values of -4 ± 2 meV and 3 ± 2 meV for the
18 redshifted and blueshifted part, respectively, with no measurable difference based on the
19 dislocation type. (For dislocations with distance to nearest neighbor below 150 nm, the
20 redshifted and blueshifted regions of both dislocations tend to overlap, making data analysis less
21 reliable in that case.) This dipole-like energy shift seems to indicate that the energy shifts may be
22 ascribed to the strain distribution around the dislocation.
23
24
25
26
27
28
29
30
31
32
33
34
35
36
37
38
39
40
41
42
43
44
45
46
47
48
49
50
51
52
53
54
55
56
57
58
59
60

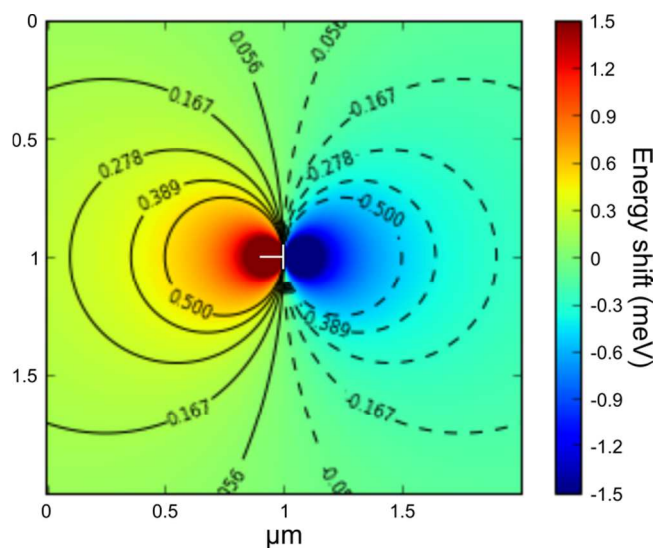


Figure 5. Simulation of the emission energy shift in the vicinity of an edge-type dislocation.

To further investigate the origin of the energy shift reported above, we conducted continuum elastic calculations to describe the strain field and emission energy shifts around an edge-type dislocation. This approach has been well-described by Gmeinwieser *et al.* to study dislocations in GaN⁴³. We thus adopted a similar approach here, for our Al_{0.46}Ga_{0.54}N sample, using the elastic constants from Ref. 44 and deformation potentials from Ref. 45 for GaN and AlN, and assuming Vegard's law applies. These calculations considered a random alloy of Al_{0.46}Ga_{0.54}N, that is, with no segregation in the vicinity of the dislocations. The results of the simulation are presented in Figure 5, where a shift of typically -1.5 meV and 1.5 meV are predicted for the tensile and compressive parts, respectively. These values are of the same order as the experimental values of -4 ± 2 meV and 3 ± 2 meV we reported. The simulations seem nevertheless to underestimate slightly the value of the emission energy shift, presumably indicating some effect of alloy segregation on the emission energy shift - *i.e.* the segregation of Ga atoms in the tensile part of the dislocation increases the (negative) energy shift, while the segregation of Al in the compressive part increases the (positive) energy shift.

In conclusion we conducted a comprehensive investigation of dislocations in AlGa_N material with an Al content $\sim 46\%$. The core configuration of the dislocations has been identified. We thus report that the dislocation core structure is in line with that of other III-Nitride alloys, but that alloying GaN with AlN tends to prevent the dissociation of mixed-type dislocations. We show that this is due to Ga and Al atoms segregation in the tensile and compressive parts of the dislocation, respectively. Finally, we investigated the optical implications of these alloy segregations. Unlike in InGa_N alloys, where In atom segregation at dislocation also occurs, the segregation of Al and Ga atoms does not significantly affect the optical properties of dislocations in AlGa_N. This study gives insights on why InGa_N-based devices are generally more resilient to dislocations than their AlGa_N-based counterparts, and brings forwards the hypothesis that doping AlGa_N with In may be an interesting approach to hinder non-radiative recombination at dislocations.

AUTHOR INFORMATION

Corresponding Author

* E-mail: fm350@cam.ac.uk

Author Contributions

The manuscript was written through contributions of all authors. All authors have given approval to the final version of the manuscript.

Notes

The authors declare no competing interest.

Funding Sources

European Research Council, European Union Seventh Framework Programme, Lindemann Trust.

ACKNOWLEDGMENT

This project is funded in part by the European Research Council under the European Community's Seventh Framework Programme (FP7/2007-2013)/ERC grant agreement No. 279361 (MACONS). The research leading to these results has received funding from the European Union Seventh Framework Programme under Grant Agreement 312483 - ESTEEM2 (Integrated Infrastructure Initiative I3). S.R. acknowledges financial support from the ERC Starting Grant 307636 "SCOPE". M.H. would like to acknowledge support from the Lindemann Trust Fellowship. Datasets for the figures in this paper can be found at <https://doi.org/10.17863/CAM.10364>.

ABBREVIATIONS

LED, light emitting diode; UV, ultra-violet; MOVPE, metal-organic vapor phase epitaxy; TMG, trimethylgallium; TMA, trimethylaluminium; TMI, trimethylindium; SiH₄, silane; NH₃, ammonia; H₂, hydrogen; N₂, nitrogen; HAADF-STEM, high-angle annular dark field scanning transmission electron microscopy; EDX, energy dispersive X-ray spectroscopy; AFM, atomic force microscopy; SEM, scanning electron microscopy; CL, cathodoluminescence; LDD, low dislocation density; HDD, high dislocation density.

REFERENCES

- (1) Nakamura, S. *Ann. Phys. (Berlin)* **2015**, 527, 335-349.
- (2) Humphreys, C.J. *MRS Bulletin* **2008**, 33, 459-470.

1
2
3
4
5
6
7
8
9
10
11
12
13
14
15
16
17
18
19
20
21
22
23
24
25
26
27
28
29
30
31
32
33
34
35
36
37
38
39
40
41
42
43
44
45
46
47
48
49
50
51
52
53
54
55
56
57
58
59
60

(3) Kneissl, M.; Rass, J. *III-Nitride Ultraviolet Emitters*; Springer: Switzerland, 2016.

(4) Narukawa, Y.; Ichikawa, M.; Sanga, D.; Sano, M.; Mukai, T. *J. Phys. D: Appl. Phys.* **2010**, *43*, 354002.

(5) Alhassan, A.I.; Farrell, R.M.; Saifaddin, B.; Mughal, A.; Wu, F.; Denbaars, S.P.; Nakamura, S.; Speck, J.S. *Opt. Express* **2016**, *24*, 17868.

(6) Davies, M.J.; Dawson, P.; Massabuau, F.C.-P.; Oehler, F.; Oliver, R.A.; Kappers, M.J.; Badcock, T.J.; Humphreys, C.J. *Phys. Status Solidi C* **2014**, *11*, 750-753.

(7) Kneissl, M.; Kolbe, T.; Chua, C.; Kueller, V.; Lobo, N.; Stellmach, J.; Knauer, A.; Rodriguez, H.; Einfeldt, S.; Yang, Z.; Johnson, N.M.; Weyers, M. *Semicond. Sci. Technol.* **2011**, *26*, 014036.

(8) Narayanan, V.; Lorenz, K.; Kim, W.; Mahajan, S. *Phil. Mag. A* **2002**, *82*, 885-912.

(9) Rhode, S.; Horton, M.; Kappers, M.; Zhang, S.; Humphreys, C.; Dusane, R.; Sahonta, S.-L.; Moram, M. *Phys. Rev. Lett.* **2013**, *111*, 025502.

(10) Rhode, S.L.; Horton, M.K.; Fu, W.Y.; Sahonta, S.-L.; Kappers, M.J.; Pennycook, T.J.; Humphreys, C.J.; Dusane, R.O.; Moram, M.A. *Appl. Phys. Lett.* **2015**, *107*, 243104.

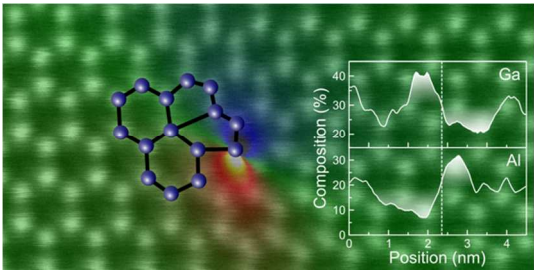
(11) Rhode, S.L.; Horton, M.K.; Sahonta, S.-L.; Kappers, M.J.; Haigh, S.J.; Pennycook, T.J.; McAleese, C.; Humphreys, C.J.; Dusane, R.O.; Moram, M.A. *J. Appl. Phys.* **2016**, *119*, 105301.

(12) Hirsch, P.B.; Lozano, J.G.; Rhode, S.; Horton, M.K.; Moram, M.A.; Zhang, S.; Kappers, M.J.; Humphreys, C.J.; Yasuhara, A.; Okunishi, E.; Nellist, P.D. *Phil. Mag.* **2013**, *93*, 3925-3938.

- (13) Yang, H.; Lozano, J.G.; Pennycook, T.J.; Jones, L.; Hirsch, P.B.; Nellist, P.D. *Nat. Com.* **2015**, *6*, 7266.
- (14) Arslan, I.; Bleloch, A.; Stach, E.A.; Browning, N.D. *Phys. Rev. Lett.* **2005**, *94*, 025504.
- (15) Horton, M.K.; Rhode, S.L.; Moram, M.A. *J. Appl. Phys.* **2014**, *116*, 063710.
- (16) Blumenau, A.T.; Elsner, J.; Jones, R.; Heggie, M.I.; Oberg, S.; Frauenheim, T.; Briddon, P.R. *J. Phys.: Condens. Matter* **2000**, *12*, 10223-10233.
- (17) Béré, A.; Serra, A. *Phys. Rev. B* **2002**, *65*, 205323.
- (18) Lee, S.M.; Belkhir, M.A.; Zhu, X.Y.; Lee, Y.H.; Hwang, Y.G.; Frauenheim, T. *Phys. Rev. B* **2000**, *61*, 16033-16039.
- (19) Belabbas, I.; Béré, A.; Chen, J.; Petit, S.; Akli Belkhir, M.; Ruterana, P.; Nouet, G. *Phys. Rev. B* **2007**, *75*, 115201.
- (20) Belabbas, I.; Chen, J.; Nouet, G. *Computational Materials Science* **2014**, *90*, 71-81.
- (21) Chen, J.; Ruterana, P.; Nouet, G. *Materials Science and Engineering* **2001**, *B82*, 117-119.
- (22) Sridhara Rao, D.V.; Kappers, M.J.; McAleese, C.; Zhu, T.; Zhu, D.; Humphreys, C.J. "Microstructural study of AlGaN/AlN buffer with 3D GaN interlayer", *XV International Workshop on Physics of Semiconductor Devices (IWPSD)* **2009**, 264-267.
- (23) Massabuau, F.C-P.; Chen, P.; Horton, M.K.; Rhode, S.L.; Ren, C.X.; O'Hanlon, T.J.; Kovács, A.; Kappers, M.J.; Humphreys, C.J.; Dunin-Borkowski, R.E.; Oliver, R.A. *J. Appl. Phys.* **2017**, *121*, 013104.

- (24) Ernst Ruska-Centre for Microscopy and Spectroscopy with Electrons. *Journal of large-scale research facilities* **2016**, 2, A43. <http://dx.doi.org/10.17815/jlsrf-2-68>.
- (25) Ernst Ruska-Centre for Microscopy and Spectroscopy with Electrons (ER-C). *Journal of large-scale research facilities*, **2015**, 1, A34. <http://dx.doi.org/10.17815/jlsrf-1-57>.
- (26) Lozano, J.G.; Yang, H.; Guerrero-Lebrero, M.P.; D'Alfonso, A.J.; Yasuhara, A.; Okunishi, E; Zhang, S.; Humphreys, C.J.; Allen, L.J.; Galindo, P.L.; Hirsch, P.B.; Nellist, P.D. *Phys. Rev. Lett.* **2014**, 113, 135503.
- (27) Massabuau, F.C.-P.; Trinh-Xuan, L.; Lodie, D.; Thrush, E.J.; Zhu, D.; Oehler, F.; Zhu, T.; Kappers, M.J.; Humphreys, C.J.; Oliver, R.A. *J. Appl. Phys.* **2013**, 113, 073505.
- (28) Drouin, D.; Hovington, P.; Gauvin, R. *Scanning* **1997**, 19, 20-28.
- (29) Muth, J.F.; Brown, J.D.; Johnson, M.A.L.; Yu, Z.; Kolbas, R.M.; Cook Jr., J.W.; Schetzina, J.F. *Mat. Res. Soc. Symp. Proc.* **1999**, 537, G5.2.
- (30) Chen, C.; Meng, F.; Song, J. *J. Appl. Phys.* **2016**, 119, 064302.
- (31) Horton, M.K.; Rhode, S.; Sahonta, S.-L.; Kappers, M.J.; Haigh, S.J.; Pennycook, T.J.; Humphreys, C.J.; Dusane, R.O.; Moram, M.A. *Nano Lett.* **2015**, 15, 923-930.
- (32) Mattila, T.; Zunger, A. *J. Appl. Phys.* **1999**, 85, 160-167.
- (33) Sakaguchi, R.; Akiyama, T.; Nakamura, K.; Ito, T. *Jpn. J. Appl. Phys.* **2016**, 55, 05FM05.
- (34) Chichibu, S.; Uedono, A.; Onuma, T.; Haskell, B.; Chakraborty, A.; Koyama, T.; Fini, P.; Keller, S.; Denbaars, S.; Speck, J.; Mishra, U.; Nakamura, S.; Yamaguchi, S.; Kamiyama, S.; Amano, H.; Akasaki, I.; Han, J.; Sota, T. *Nat. Mater.* **2006**, 5, 810-816.

- (35) Liu, Q.; Lu, J.; Gao, Z.; Lai, L.; Qin, R.; Li, H.; Zhou, J.; Li, G. *Phys. Status Solidi B* **2010**, *247*, 109-114.
- (36) Schulz, S.; Marquardt, O.; Coughlan, C.; Caro, M.A.; Brandt, O.; O'Reilly, E.P. *Proc. of SPIE* **2015**, *9357*, 93570C.
- (37) Sugahara, T.; Sato, H.; Hao, M.; Naoi, Y.; Kurai, S.; Tottori, S.; Yamashita, K.; Nishino, K.; Romano, L.T.; Sakai, S. *Jpn. J. Appl. Phys.* **1998**, *37*, L398-L400.
- (38) Cherns, D.; Henley, S.J.; Ponce, F.A. *Appl. Phys. Lett.* **2001**, *78*, 2691-2693.
- (39) Rosner, S.J.; Carr, E.C.; Ludowise, M.J.; Girolami, G.; Erikson, H.I. *Appl. Phys. Lett.* **1997**, *70*, 420-422.
- (40) Onuma, T.; Chichibu, S.F.; Uedono, A.; Sota, T.; Cantu, P.; Katona, T.M.; Keadig, J.F.; Keller, S.; Mishra, U.K.; Nakamura, S.; DenBaars, S.P. *J. Appl. Phys.* **2004**, *95*, 2495-2504.
- (41) Nepal, N.; Li, J.; Nakarmi, M.L.; Lin, J. Y.; Jiang, H.X. *Appl. Phys. Lett.* **2006**, *88*, 062103.
- (42) Rigutti, L.; Mancini, L.; Lefebvre, W.; Houard, J.; Hernández-Maldonado, D.; Di Russo, E.; Giraud, E.; Butté, R.; Carlin, J.-F.; Grandjean, N.; Blavette, D.; Vurpillot, F. *Semicond. Sci. Technol.* **2016**, *31*, 095009.
- (43) Gmeinwieser, N.; Schwarz, U.T. *Phys. Rev. B* **2007**, *75*, 245213.
- (44) Vurgaftman, I.; Meyer, J.R. *J. Appl. Phys.* **2003**, *94*, 3675-3696.
- (45) Yan, Q.; Rinke, P.; Janotti, A.; Scheffler, M.; Van de Walle, C.G. *Phys. Rev. B* **2014**, *90*, 125118.



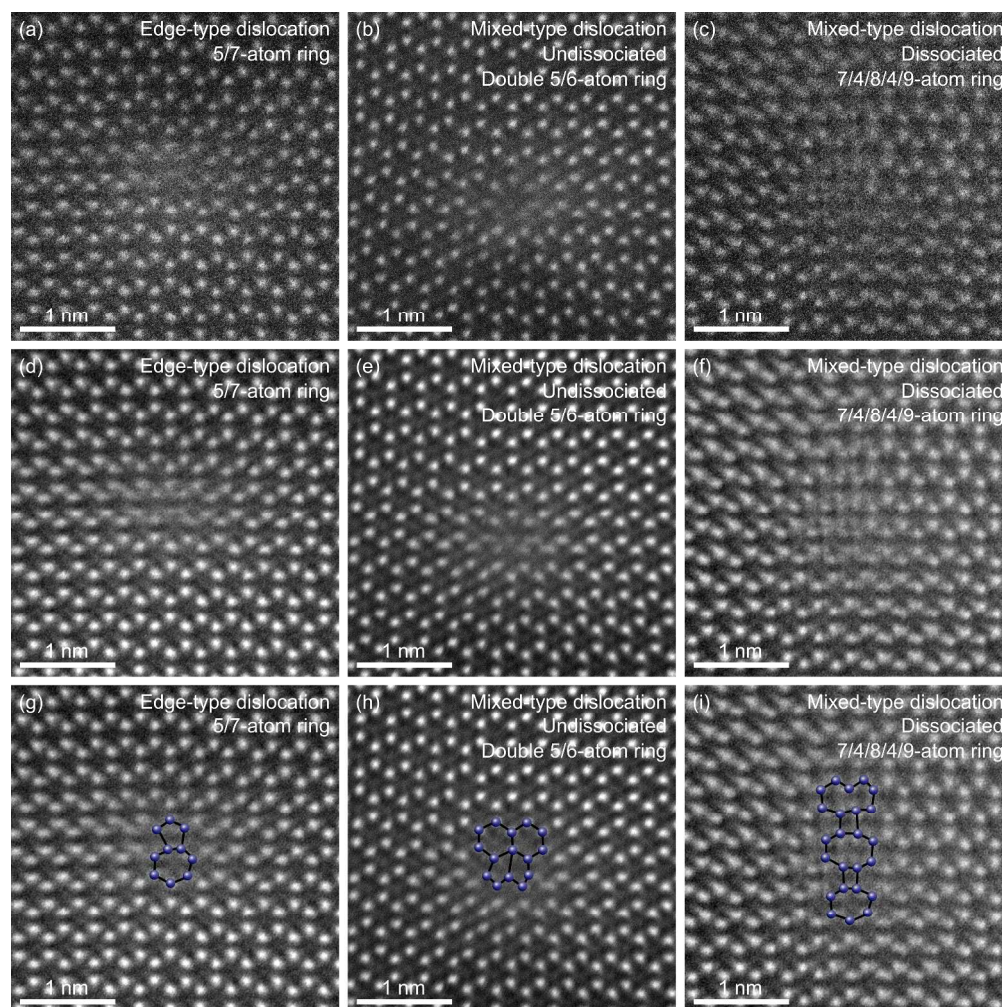


Figure 1. Plan-view aberration-corrected HAADF-STEM image of the AlGaN sample, showing the core structure of an edge-type dislocation (5/7-atom ring)(a,d,g), an undissociated mixed-type dislocation (double 5/6-atom ring)(b,e,h) and a dissociated mixed-type dislocation (7/4/8/4/9-atom ring)(c,f,i). Raw unfiltered images (a-c), and ABSF-filtered (average background subtraction filter) (d-f) with atomic columns identified to guide the eye (g-i).

1111x1110mm (96 x 96 DPI)

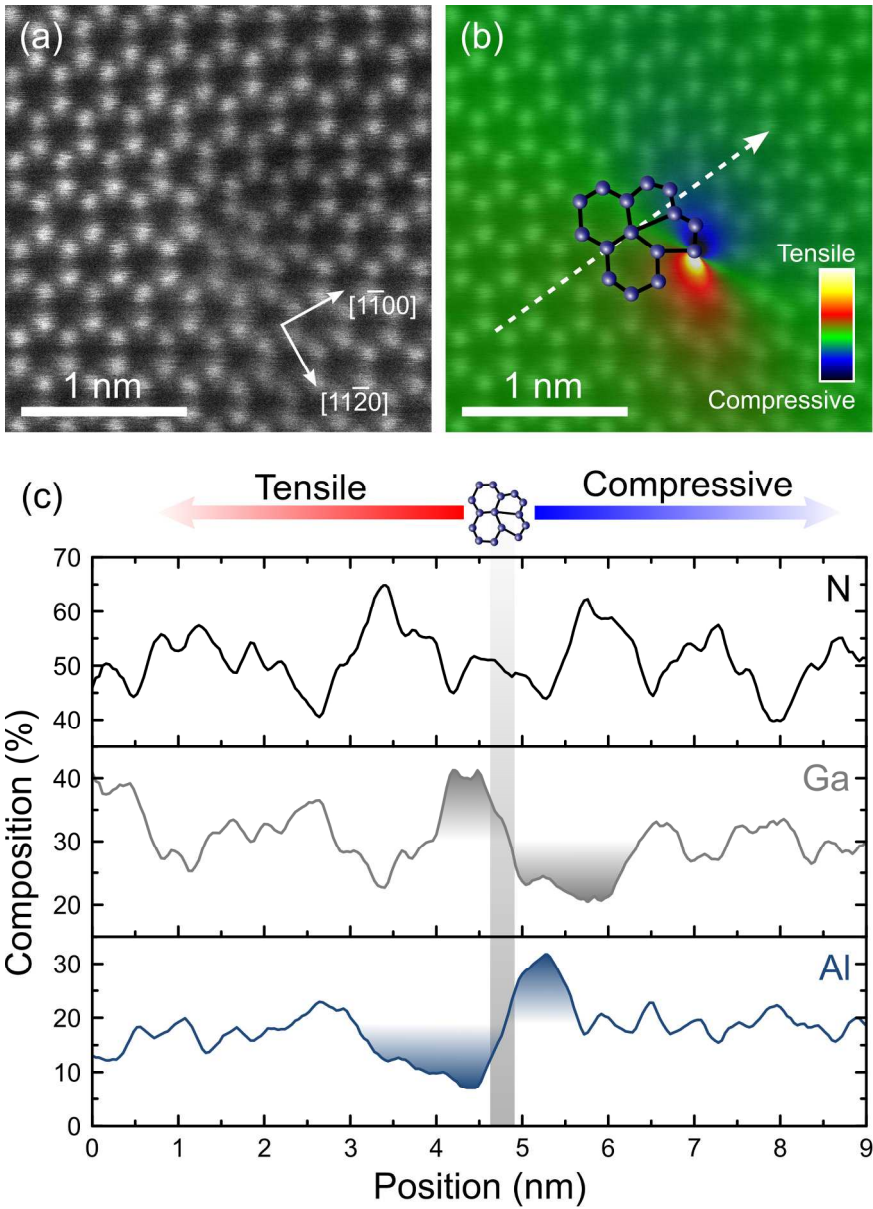


Figure 2. (a) Unfiltered HAADF-STEM image of an undissociated mixed-type dislocation. (b) ABSF-filtered image of (a) with geometric phase analysis overlay showing the x-x strain component (x-axis parallel to $[11\bar{2}0]$). (c) EDX line scan showing the composition of Al, Ga, and N along the line depicted in (b) (with a ca. 1 nm analysis width).

528x731mm (96 x 96 DPI)

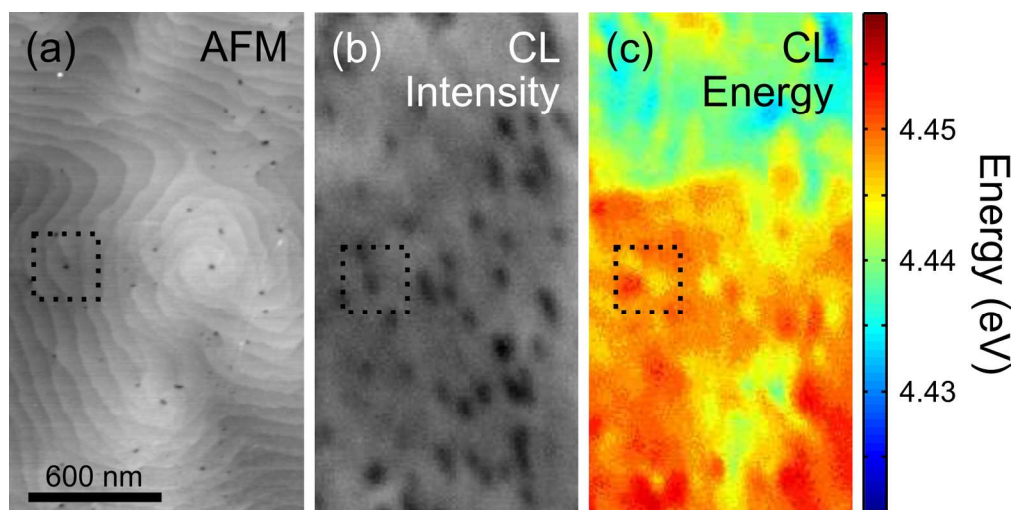


Figure 3. (a) AFM, (b) CL integrated intensity, and (c) CL peak emission energy of the same region in the AlGaIn sample.

528x265mm (96 x 96 DPI)

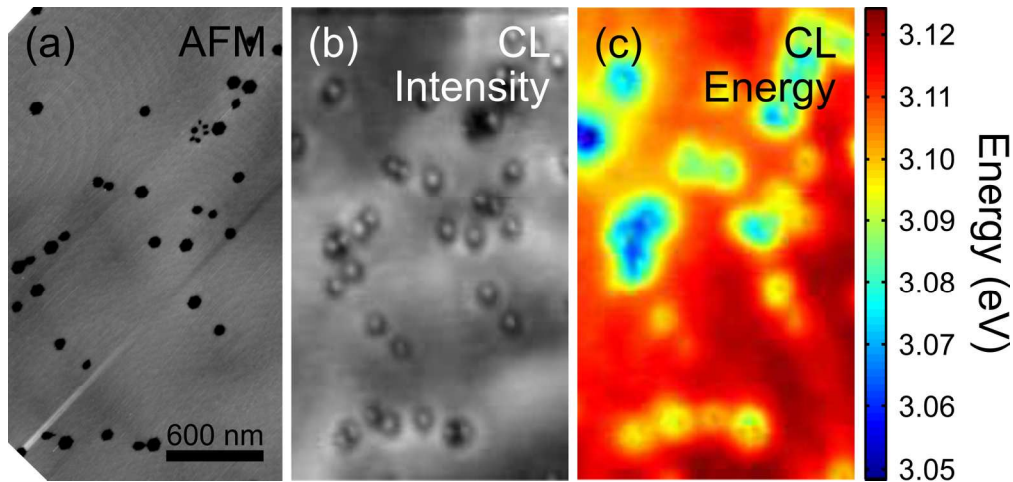


Figure 4. (a) AFM, (b) CL integrated intensity, and (c) CL peak emission energy of the same region in the InGaN sample.

528x250mm (96 x 96 DPI)

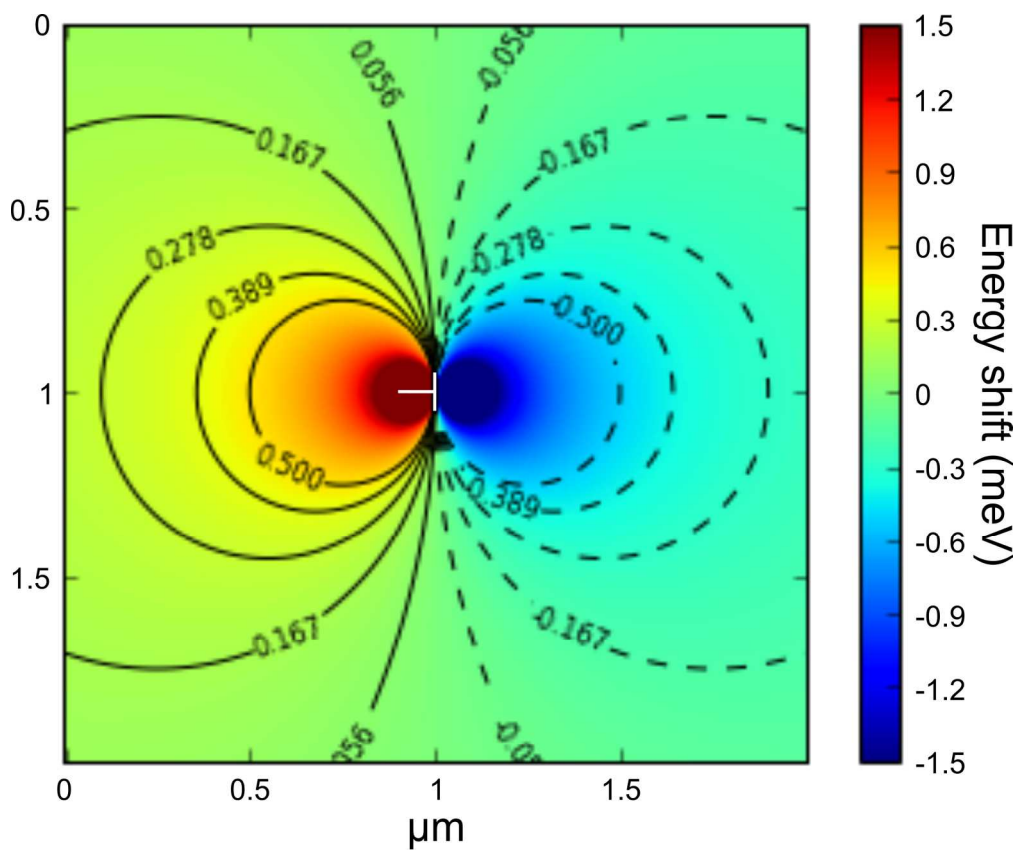


Figure 5. Simulation of the emission energy shift in the vicinity of an edge-type dislocation.

528x441mm (96 x 96 DPI)

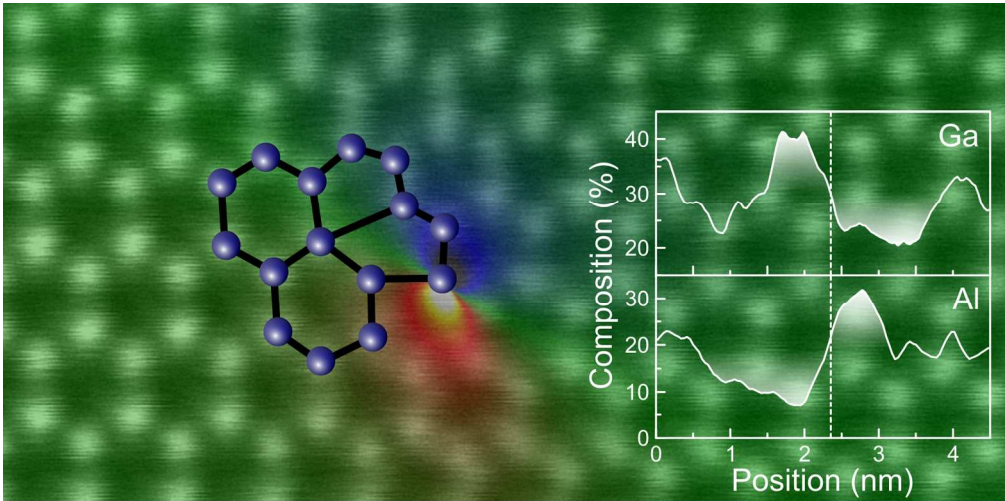


Table of Content Graphic

500x249mm (96 x 96 DPI)